Nanoscale Advances

ROYAL SOCIETY OF CHEMISTRY

PAPER

View Article Online
View Journal | View Issue

Cite this: *Nanoscale Adv.*, 2024, **6**, 697

Synthesis and enhanced room-temperature thermoelectric properties of CuO–MWCNT hybrid nanostructured composites

Raitis Sondors,[a] Davis Gavars,[a] Elmars Spalva,[b] Artis Kons,[c] Rynno Lohmus,[d] Margarita Volkova,[a] Raimonds Meija[b] and Jana Andzane*[a]

This work presents the synthesis of novel copper oxide–multiwalled carbon nanotube (CuO–MWCNT) hybrid nanostructured composites and a systematic study of their thermoelectric performance at near-room temperatures as a function of MWCNT wt% in the composite. The CuO–MWCNT hybrid nanostructured composites were synthesized by thermal oxidation of a thin metallic Cu layer pre-deposited on the MWCNT network. This resulted in the complete incorporation of MWCNTs in the nanostructured CuO matrix. The thermoelectric properties of the fabricated CuO–MWCNT composites were compared with the properties of CuO–MWCNT networks prepared by mechanical mixing and with the properties of previously reported thermoelectric $[CuO]_{99.9}[SWCNT]_{0.1}$ composites. CuO–MWCNT hybrid composites containing MWCNTs below 5 wt% showed an increase in the room-temperature thermoelectric power factor (PF) by ~2 times compared with a bare CuO nanostructured reference thin film, by 5–50 times compared to mixed CuO–MWCNT networks, and by ~10 times the PF of $[CuO]_{99.9}[SWCNT]_{0.1}$. The improvement of the PF was attributed to the changes in charge carrier concentration and mobility due to the processes occurring at the large-area CuO–MWCNT interfaces. The Seebeck coefficient and PF reached by the CuO–MWCNT hybrid nanostructured composites were 688 μV K^{-1} and ~4 μW m^{-1} K^{-2}, which exceeded the recently reported values for similar composites based on MWCNTs and the best near-room temperature inorganic thermoelectric materials such as bismuth and antimony chalcogenides and highlighted the potential of CuO–MWCNT hybrid nanostructured composites for applications related to low-grade waste heat harvesting and conversion to useable electricity.

Received 15th October 2023
Accepted 15th December 2023

DOI: 10.1039/d3na00888f

rsc.li/nanoscale-advances

Introduction

The generation of waste heat is an inevitable companion of modern society. A significant portion of the waste loss is from near-room temperature domestic applications such as hot pipes and chimneys, as well as imperfect thermal insulation of buildings. Considering the ever-increasing demand for renewable energy, capturing and transforming waste heat into reusable energy are important. This can be done using the thermoelectric (TE) effect, a well-known property of semiconductor materials, which directly converts heat to electricity without moving parts.[1] The efficiency of TE materials and devices is characterized by a dimensionless figure of merit $ZT = S^2\sigma T k^{-1}$, where S is the Seebeck coefficient, σ is the electrical conductivity of the material, T is the measurement temperature, and k is the thermal conductivity of the material. ($S^2\sigma$) is usually referred to as the material's thermoelectric power factor (PF). The well-known high-performance materials for near-room temperature applications are chalcogenides such as bismuth, antimony, tin and lead tellurides, and selenides.[2] However, these materials are rigid and easily degrade due to their rapid oxidation in air.[3] This hampers their application for low-grade waste heat harvesting from non-linear surfaces, as well as in wearable devices, which is a rapidly developing field in the area of thermoelectrics.[4,5] Recently, an approach of combining these materials with single- (SWCNTs)[6] or multiwall (MWCNTs)[7,8] carbon nanotubes has been reported. SWCNT–Bi_2Te_3 composites showed a remarkable PF of 1.6 mW m^{-1} K^{-2} and ZT of 0.89.[6] However, it should be noted that such materials are susceptible to oxidation in air, resulting in degradation of their properties, and require preservation. The approach of encapsulation in a non-conductive polymer for the preservation of their properties and application in flexible TE devices for domestic waste heat harvesting has been demonstrated for MWCNT–Bi_2Se_3 and MWCNT–Sb_2Te_3 hybrid networks, showing PF in a range of ~0.4–10 μW m^{-1} K^{-2} and generating output power reaching 10

[a]*Institute of Chemical Physics, University of Latvia, Raina blvd. 19, Riga, Latvia, LV-1586. E-mail: jana.andzane@lu.lv*
[b]*3D Strong Ltd, Instituta Str. 36-17, Ulbroka, Latvia, LV-2130*
[c]*Faculty of Chemistry, University of Latvia, Raina blvd. 19, Riga, Latvia, LV-1586*
[d]*Institute of Physics, University of Tartu, W. Ostwaldi 1, 50411, Tartu, Estonia*

μW cm^{-2}, which is comparable to state-of-the-art micro- and nano-power thermoelectric generators for low-grade heat conversion.[7] However, the rarity, high price, susceptibility to the environmental impact, and toxicity of these materials still make them not the best choice for domestic applications.

The alternative group of materials for TE applications is metal oxides, as they are abundant, low-cost, easily processable by scalable environmentally friendly methods, and chemically stable in air and at high temperatures.[9,10] In this group, copper oxide plays an important role. It is an intrinsically p-type semiconductor, which can be easily obtained in the form of thin films, nanowires, or nanoparticles *via* the thermal oxidation process of copper[11–14] or the chemical route.[15,16] CuO nanostructures on their own or combined with carbon nanotubes are widely studied for a wide range of applications such as sensing,[17] photocatalysts for degradation of toxic contaminants,[18] hydrogen production and CO_2 reduction,[19] as electrodes in batteries and supercapacitors,[18,20] in solar power applications,[21,22] *etc.* However, despite a high Seebeck coefficient of ~630 μV K^{-1} reported for commercially available CuO powder,[23] the study of the application of CuO in TE devices is limited to a few reports. The limiting factor for the application of CuO in thermoelectrics is the low electrical conductivity of this material (~1.5×10^{-4} S cm^{-1}), resulting in a low PF being in the order of ~10^{-4} μW m^{-1} K^{-2} for commercially available pure CuO powder.[23] The attempt to use obtained by thermal oxidation method CuO nanowires instead of the commercially available CuO powder showed that the CuO nanowires-based TE module may reach as high Seebeck coefficient as 820 μV K^{-1}. However, shown by this TE module PF was 0.37 μW m^{-1} K^{-2} due to the low electrical conductivity of the nanowire network.[12] In contrast, joining together chemically obtained CuO nanoparticles and SWCNTs in composite materials by mixing and sonication approaches resulted in a remarkable Seebeck coefficient of 882 μV K^{-1} and PF of 2500 μW m^{-1} K^{-2}, but for the measurement temperature of 673 K, while room-temperature measurements of these CuO–SWCNT composites showed Seebeck coefficients below 150 μV K^{-1} and a PF of ~0.45 μW m^{-1} K^{-2}, thus indicating not good enough TE performance of these composites for domestic waste harvesting applications.

This work presents a three-step approach to fabricating novel CuO–MWCNT hybrid nanostructured composites for application in near-room temperature thermoelectrics as low-grade waste heat capturing and converting materials to useful energy. The CuO–MWCNT hybrid composites with different mass ratios are fabricated by a thin metallic Cu layer deposition over the MWCNT network, followed by thermal oxidation of the Cu–MWCNT structure until a complete transition of Cu to CuO. The thermoelectric performance of the obtained CuO–MWCNT hybrid composites was compared with that of the pure CuO nanostructured thin film and with that of CuO–MWCNT networks prepared by mechanical mixing and sonication of pre-synthesized *via* thermal oxidation CuO nanowires and MWCNTs. This study revealed that the thermoelectric performance of the CuO–MWCNT hybrid composites prepared using the presented method showed nearly an order of magnitude higher PF compared to the abovementioned CuO–SWCNT composite and have potential for the further increase of the PF, proving their potential for application in near-room temperature thermoelectrics.

Materials and methods

Synthesis of MWCNTs and fabrication of MWCNT networks

MWCNTs were synthesized using the spray-assisted chemical vapour deposition method from a gas phase as described elsewhere.[24] The synthesis occurred in an inert (argon) atmosphere under atmospheric pressure at a flow rate of 20 mm s^{-1}. 2 wt% ferrocene dissolved in toluene was used for one synthesis cycle. The synthesis was carried out for 60 min at a temperature of 800 °C.

Synthesis of CuO nanowires and fabrication of mixed CuO–MWCNT networks

CuO nanowires were synthesized as described elsewhere.[11] Briefly, CuO nanowires were synthesized by thermal oxidation of 25 μm Cu foil pieces (99.9%, Goodfellow GmbH, Hamburg, Germany) at 500 °C in air and under an external electrical field applied by two electrodes not electrically connected to the Cu foil pieces subjected to oxidation. The oxidized Cu foil was sonicated in isopropyl alcohol in an ultrasonic bath (Sonorex RK 100, BANDELIN electronic GmbH & Co. KG, Berlin, Germany) at a frequency of 35 kHz and power of 320 W for 5–10 s to separate the CuO nanowires from the residues of the Cu substrate and suspend them for the further use. For the fabrication of mixed CuO–MWCNT networks, CuO nanowires and MWCNTs in desired mass ratios (0.05, 0.5 and 20 wt% of MWCNTs) were sonicated in isopropyl alcohol in an ultrasonic bath for 10 min and drop-cast on a solid substrate (glass slide) and dried in ambient air. Electrodes were fabricated using silver paint (Ted Pella, Inc., Redding, CA, USA). The distance between the electrodes was 5 mm, and the width of the samples was 10 mm.

Fabrication of CuO–MWCNT hybrid nanostructured composites

First, MWCNT networks were deposited on glass substrates using the spray-coating method. The prepared MWCNT networks were coated with a 500 nm layer of metallic Cu using the thermal evaporation method under vacuum conditions (SAF EM, Sidrabe AS, Riga, Latvia). The fabricated Cu–MWCNT network was thermally oxidized in air at 500 °C for 4 hours using a single-zone quartz tube furnace (GSL-1100X, MTI Corp., Richmond, CA, USA) to achieve a complete transition of Cu to CuO. For the reference bare CuO sample, a 500 nm thin layer of metallic Cu was deposited on a glass substrate and oxidized. CuO–MWCNT hybrid composites with MWCNT wt% of 0.36, 0.9, 1.8, 3.6, 9, and 18 were fabricated. Electrodes were made using silver paint similar to the mixed CuO–MWCNT samples.

Morphological and structural characterization

The morphology of the samples was studied using a field-emission scanning electron microscope (SEM) Hitachi-4800

(Hitachi Ltd., Tokyo, Japan), using an electron beam energy of 5 kV, and a high-resolution transmission electron microscope (HR-TEM FEI Titan Themis 200, FEI Company, Hillsboro, OR, USA), using an electron beam energy of 200 kV. For the structural characterization of the samples, X-ray diffraction patterns were obtained using an X-ray diffractometer (XRD) Bruker D8 Discover (Bruker Corp., Billerica, MA, USA). For the identification of the diffraction peaks, the ICDD database PDF-2/Release 2021 was used (ref. cards PDF 01-073-6023 CuO).

Electrical and thermoelectric characterization

The current–voltage curves of the samples were recorded using a Keithley 6487 picoammeter/voltage source. To determine the Seebeck coefficient, a lab-made device reported elsewhere[25] and calibrated using the NIST Standard Reference material 3451 (NIST, Gaithersburg, MD, USA) for a low-temperature Seebeck coefficient was used at room temperature under ambient conditions. The thermoelectric voltage generated by the sample was measured using a HP 34401A multimeter (Hewlett-Packard Company, Palo Alto, CA, USA) and custom software for automatic data recording. The temperature gradient between the sample sides did not exceed 10% of the absolute temperature at which the measurements were performed. The thermoelectric voltage generated by the samples before was calculated as the mean of twenty consecutive measurements at each temperature difference, and ±standard deviation [SD] was estimated from these twenty measurements.

Results and discussion

CuO–MWCNT hybrid nanostructured composites were fabricated using a three-step process (Fig. 1a–d).

First, MWCNT networks were prepared onto glass substrates using the spray-coating method (Fig. 1a-1); next, a Cu layer with a thickness of 500 nm was deposited over a prefabricated MWCNT network. The observation of the initial stage of Cu deposition (first 100 nm of Cu was deposited on the MWCNT network using the thermal evaporation method) revealed that initially Cu uniformly deposits on the surfaces of MWCNTs, forming shells around them (Fig. 1b-2). Images obtained using scanning transmission electron microscopy (STEM) confirmed that initially Cu deposits on the surfaces of MWCNTs in the form of islands (Fig. 2a), which further coalesce together as illustrated in Fig. 1b.

The HRTEM images of the Cu–MWCNT sample (Fig. 2b and c) revealed the polycrystalline nature of the deposited Cu nanoislands and their direct contact with the MWCNTs. Further Cu deposition filled the gaps between the MWCNTs and Cu, forming a continuous film with embedded MWCNTs (Fig. 1c-2). The XRD patterns obtained for the Cu–MWCNT network showed the presence of high-intensity peaks at a 2-degree theta of 43.3 and 50.4, corresponding to the (111) and (200) planes of Cu, respectively (Fig. 2g). The presence of oxide was not detected. After the thermal oxidation, the MWCNTs remained embedded in the nanostructured CuO layer, consisting of CuO nanoparticles and nanowires (Fig. 1d-3), which are usually formed on the surface of thermally oxidized in air Cu[11,13] and are not related to the presence of MWCNTs within the Cu layer. The STEM image of the oxidized Cu–MWCNT sample revealed the presence of Cu and O, indicating oxidation of Cu (Fig. 2d). The HRTEM images of the oxidized Cu–MWCNT showed that fragments of MWCNTs that have preserved their structure are closely bonded with the crystalline CuO nanostructures (Fig. 2e and f), presumably due to the formation of Cu–O–C bonds between the CuO coating layer and the outer surfaces of MWCNTs during the thermal oxidation process.[26] The complete oxidation of Cu to CuO was proved by the XRD patterns obtained for the oxidized Cu–CNT samples (Fig. 2h). The XRD patterns showed high-intensity peaks at a 2-degree theta of 35.5 and 38.8 related to the (002) and (111) crystallographic planes of CuO, respectively, indicating its highly crystalline structure. The detected lower-intensity peaks at 32.5, 48.8, 53.5, 58.5, 61.5, 62.2, and 68.2 (Fig. 2h) are characteristic of the monoclinic phase of CuO nanostructures. No additional peaks were observed, indicating the absence of commonly present CuO impurities such as Cu_2O[27] or $Cu(OH)_2$.[28] This proves the high crystallinity and purity of the synthesized CuO nanostructures, which aligns with the previously reported crystalline structure and purity of CuO nanoparticles grown on graphene.[29] The oxidized Cu–MWCNT samples forming hybrid structures will be referred to as CuO–CNT hybrid composites. For the comparison

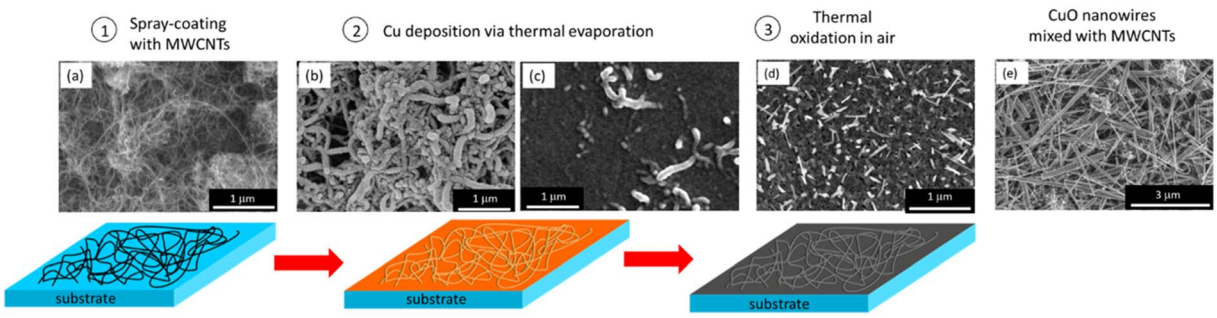

Fig. 1 Schematics and representative scanning electron microscope images of (a-1) a MWCNT network used as a substrate for Cu layer deposition; (b-2) initial 100 nm thin Cu layer deposited on the MWCNT network; (c-2) 500 nm thin Cu layer deposited on the MWCNT network; (d-3) CuO–MWCNT composite fabricated by thermal oxidation of the Cu–MWCNT network (containing ~2 wt% MWCNTs); (e) CuO–MWCNT network prepared by mechanical mixing of CuO nanowires with MWCNTs (containing 0.5 wt% MWCNTs).

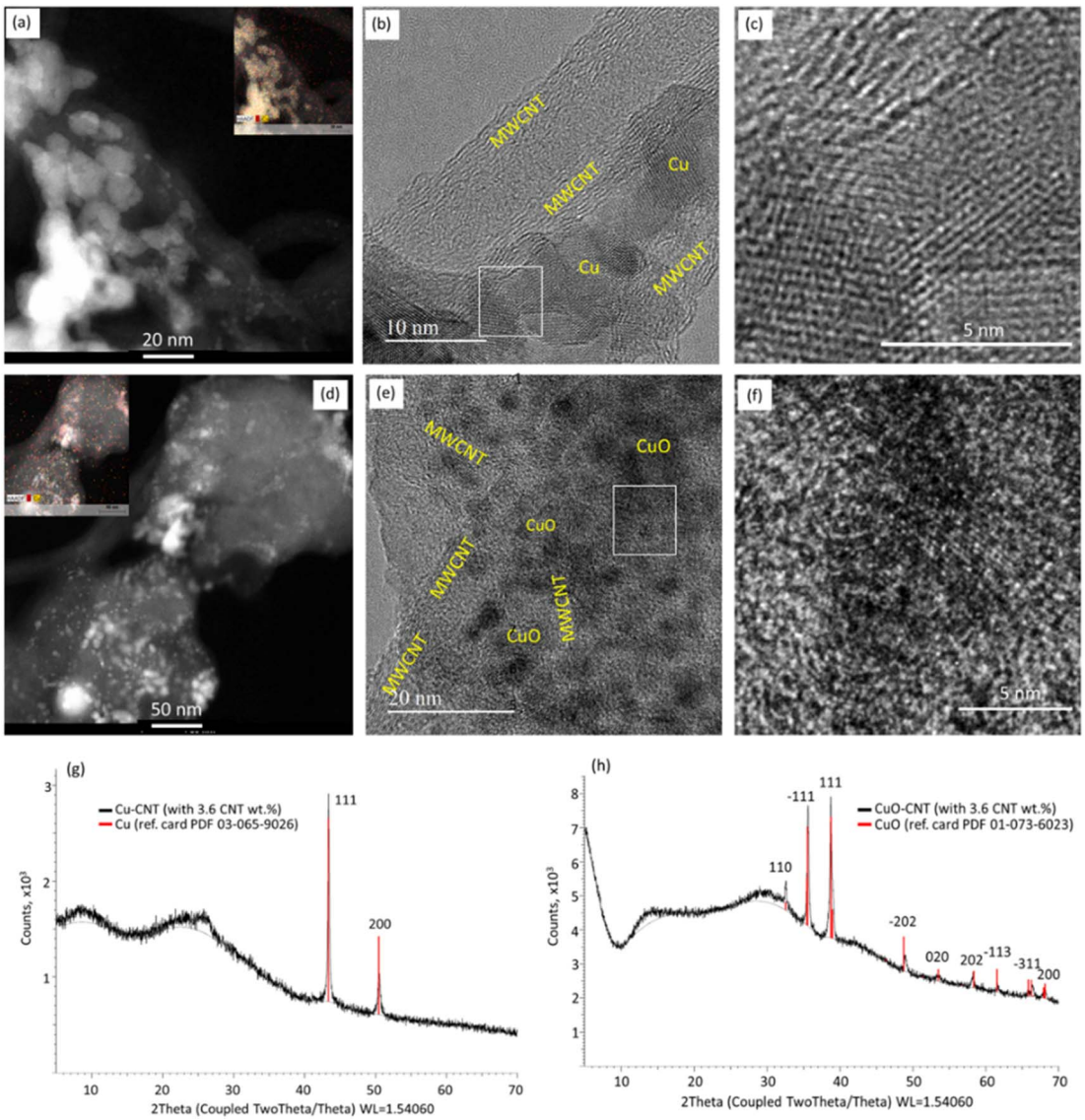

Fig. 2 (a, d) Scanning transmission electron microscopy (STEM) images of (a) Cu–MWCNT and (d) CuO–MWCNT samples; insets – mapping images illustrating the presence of Cu and O in the samples; (b and e) high-resolution transmission electron microscopy (HRTEM) images of (b) Cu–MWCNT and (e) CuO–MWCNT samples; (c and f) close view of the squared areas in (b) and (e) respectively; (g and h) X-ray diffraction patterns obtained for (g) Cu–MWCNT and (h) CuO–MWCNT samples.

of properties, CuO–MWCNT networks were prepared by mechanical mixing of CuO nanowires, obtained *via* thermal oxidation of Cu in the air, and MWCNTs, as shown in Fig. 1e. It is seen that, in that case, the MWCNTs and CuO nanowires form a randomly oriented network with multiple mechanical and electrical contacts between the network components. These samples will be referred to in the text as CuO–MWCNT mixed networks.

The current–voltage (*I*–*V*) curves of both types of CuO–MWCNT samples showed linear behaviour for all ratios of MWCNT wt% in them (Fig. 3a).

Linear *I*–*V* curves indicate well-established electrical contacts between the network and composite components throughout the sample. However, it is seen from Fig. 3a and Table 1 that despite the four times lower content of MWCNTs in the CuO–MWCNT mixed network (0.5 wt% MWCNTs) compared to the CuO–MWCNT hybrid composite (~2 wt% MWCNTs), the electrical conductivity of the mixed sample (~60 S cm^{-1}) is by a factor of 7.5 higher than that of the hybrid sample (~8 S cm^{-1}).

The higher electrical conductivity of the mixed CuO–MWCNT network may indicate that the main conductance path in this type of sample is through the established MWCNT network. In contrast, in the CuO–MWCNT hybrid composites, the electrical conductance most likely occurs through the CuO nanostructures as the MWCNTs are surrounded by the nanostructured CuO during the fabrication process (Fig. 1b–d). This hypothesis is supported by the data on electrical conductivity σ obtained for the mixed CuO–MWCNT networks containing low (0.05 wt%) and relatively high (20 wt%) amounts of MWCNTs

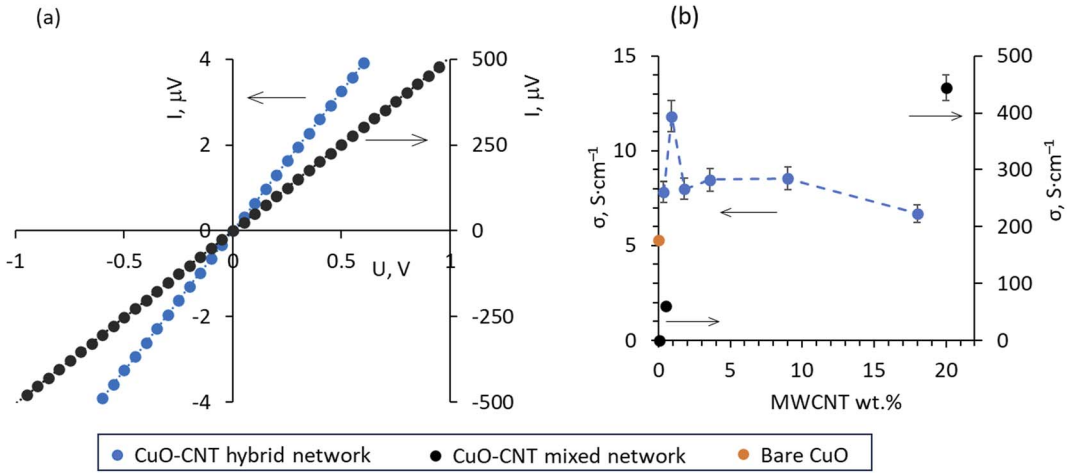

Fig. 3 (a) Representative current–voltage curves of the CuO–MWCNT hybrid composite with ~2 wt% MWCNTs (blue dots, primary axis) and the CuO–MWCNT mixed network with 0.5 wt% MWCNTs (black dots, secondary axis); (b) electrical conductivity of the bare CuO layer (orange dot), CuO–MWCNT hybrid composites (blue dots), and CuO–MWCNT mixed networks (black dots, secondary axis) *vs.* MWCNT wt% in the network.

(Fig. 3b, Table 1). For the mixed CuO–MWCNT network containing 0.05 wt% MWCNTs, the σ was very low (5×10^{-3} S cm^{-1}), which most likely indicates that the MWCNT content was insufficient to establish a well-conductive network, and the conductance occurred partially through the MWCNTs and partially through the CuO nanowires (Fig. 1e). It should be noted that such a low conductivity is in line with the previously reported data for the networks prepared from the as-synthesized CuO nanowires by the drop-cast method[27] and supports the hypothesis that in the mixed CuO–MWCNT network containing 0.05 wt% MWCNTs the conductive MWCNT network throughout the sample was not formed. At the same time, the σ of the mixed CuO–MWCNT network containing 20 wt% MWCNTs was the highest among all the tested samples (444 S cm^{-1}), proving the establishment of a conductive MWCNT network as the main conduction path in the mixed CuO–MWCNT networks. In contrast, the σ of the CuO–MWCNT hybrid composites was roughly by a factor of 1.5–2 higher compared to that of bare CuO ($\sigma = 5.3$ S cm^{-1}) and varied within a relatively narrow range between ~7 and ~12 S cm^{-1} (Fig. 3b, Table 1). This points to the different conduction mechanisms in the hybrid CuO–MWCNT composites: most likely, the electrical conductance occurs through the CuO nanostructures, forming hybrid structures with the MWCNT fragments (Fig. 2e), preventing direct electrical contacts between the MWCNTs and formation of a highly conductive MWCNT network. In that case, the content of the MWCNTs in the CuO–MWCNT hybrid composite does not play such a significant role as in the case of the mixed networks. However, the fragments of MWCNTs in the hybrid composites may contribute to the total conductance of the samples, providing highly conductive channels connecting the CuO nanostructures (Fig. 2e). The variations in σ may be related to the changes in the charge carrier concentration caused by the charge (electron) transfer from CuO to MWCNTs

Table 1 Room-temperature resistance (R), charge carrier concentration (n), mobility (μ), electrical conductivity (σ), Seebeck coefficient (S), and power factor (PF) of CuO–CNT hybrid composites and mixed networks containing different wt% of MWCNTs

Sample type	MWCNT wt%	R, kΩ	n, $\times 10^{20}$, cm^{-3}	μ, $\times 10^{-3}$, cm^2 V^{-1} s^{-1}	σ, $\times 10^{-2}$, S cm^{-1}	S, μV K^{-1}	PF, μW m^{-1} K^{-2}
Bare CuO	0	227.4 ± 0.2	0.73	4.5	5.3 ± 0.1	632 ± 30	2.1 ± 0.2
CuO–MWCNT hybrid	0.36	153.4 ± 0.1	1.02	4.8	7.8 ± 0.1	503 ± 25	2 ± 0.2
CuO–MWCNT hybrid	0.9	101.4 ± 0.1	1.05	7	11.8 ± 0.2	495 ± 25	2.9 ± 0.3
CuO–MWCNT hybrid[a]	1.8	50.1 ± 0.1	0.63	8	8.05 ± 0.05	688 ± 35	3.8 ± 0.4
CuO–MWCNT hybrid	3.6	141.4 ± 0.1	0.81	6.5	8.50 ± 0.05	589 ± 30	2.9 ± 0.4
CuO–MWCNT hybrid	9	140.6 ± 0.1	1.15	4.6	8.45 ± 0.05	464 ± 23	1.8 ± 0.2
CuO–MWCNT hybrid	18	179.2 ± 0.2	1.12	3.77	6.75 ± 0.05	475 ± 25	1.5 ± 0.1
CuO–MWCNT mixed	0.05	24 000 ± 100	—	—	0.005 ± 0.001	30 ± 15	(8 ± 1)·10^{-6}
CuO–MWCNT mixed	0.5	2.0 ± 0.05	—	—	60.0 ± 0.1	40 ± 5	0.08 ± 0.01
CuO–MWCNT mixed	20	0.27	—	—	444 ± 5	35 ± 5	0.7
$[CuO]_{99.9}[SWCNT]_{0.1}$[30]	0.1	—	—	—	~20	~150	0.45
CuO nanowires[12]	—	—	—	—	~0.55–2	430–820	0.37
Sb_2Te_3–MWCNT hybrid networks[7]	7–25	0.2–2	—	—	385–700	40–60	~2.5

[a] The sample before the oxidation consisted of 3 consecutively deposited Cu–CNT layers; the MWCNT wt% is given per one layer.

under non-equilibrium conditions (*i.e.*, when the external heat is supplied to the sample).[30] It was observed that the presence of ~1 wt% MWCNTs resulted in the most significant enhancement of the electrical conductivity (Fig. 3b, Table 1), presumably due to the optimal ratio of the CuO–MWCNT surface area and reduced thermal diffusivity of the MWCNTs in the CuO layer, allowing a maximum number of electron holes to be contributing to the conductance, similarly to that reported for CuO/SWCNT composites.[30]

The different main conductance paths in mixed CuO–MWCNT networks and hybrid composites are proved by the values of Seebeck coefficients determined from the measurements of thermally generated voltage U_T, measured *vs.* temperature difference ΔT applied to the samples (Fig. 4a, Table 1).

The Seebeck coefficient values of hybrid CuO–MWCNT composites with different contents of MWCNTs varied in the range from 464 to 688 μV K^{-1} (Fig. 4b, Table 1), which is comparable with the Seebeck coefficient values reported for CuO and proves the dominating contribution of CuO nanostructures to the thermoelectric performance of the hybrid CuO–MWCNT composites. Seebeck coefficient values allow the evaluation of charge carrier concentration and mobility in the material using the Mott relation:[31]

$$S = \frac{8\pi^2 k_B{}^2 T}{3eh^2} m^* \left(\frac{\pi}{3n}\right)^{\frac{2}{3}}, \quad (1)$$

where S is the Seebeck coefficient, k_B is Boltzmann's constant, e is the electron charge, h is Planck's constant, T is the absolute measurement temperature, m^* is the effective mass of the carrier ($m^* = 7.9m_0$ for the hole in CuO[32]), and m_0 is the electron mass. In turn, the charge carrier mobility may be calculated using the following equation:

$$\mu = \frac{\sigma}{ne}, \quad (2)$$

where μ is the charge carrier mobility, σ is the electrical conductivity, n is the charge carrier concentration, and e is the electron charge. The estimated charge carrier concentrations using eqn (1) for the hybrid CuO–MWCNT composites were in the order of ~10^{20} cm^{-3} and showed a tendency to increase compared to bare CuO when the MWCNT content was below 1 wt% and then decrease when the MWCNT content was

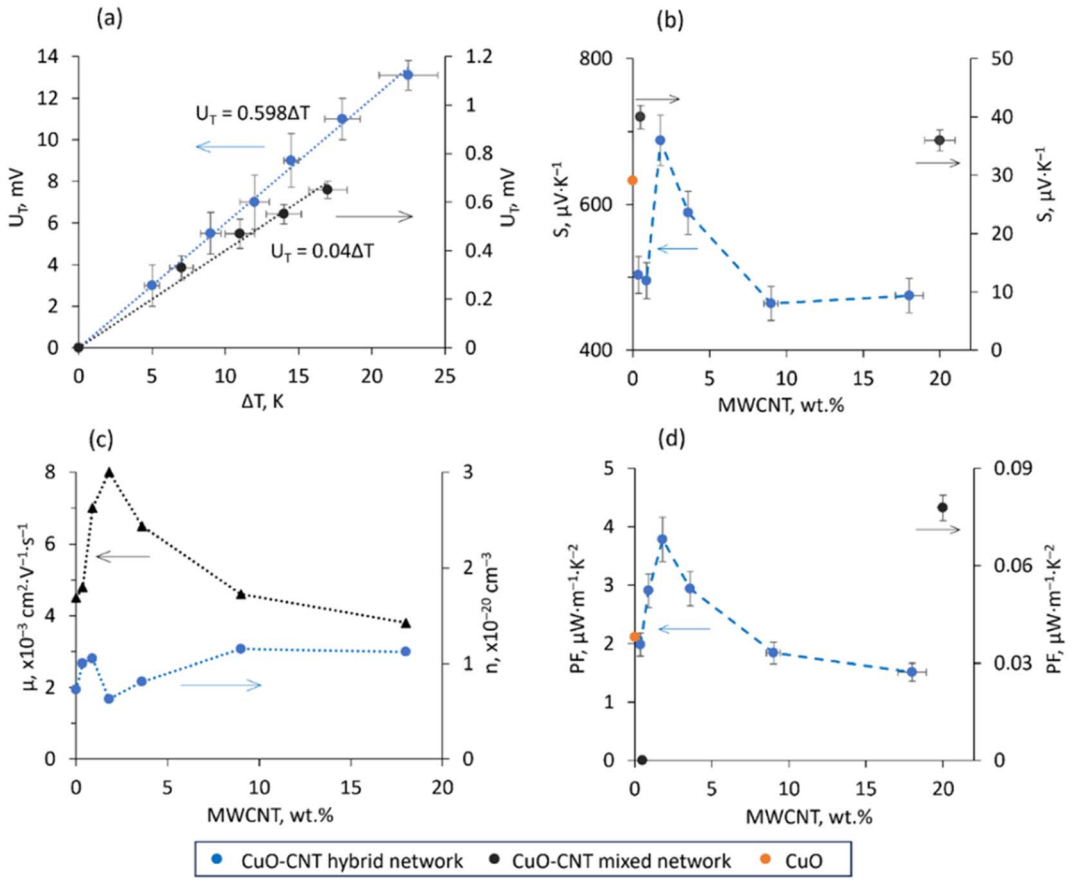

Fig. 4 (a) Thermally generated voltage U_T *vs.* temperature difference applied between the sides of the CuO–MWCNT hybrid composite (3.6 wt% MWCNTs, blue dots, primary axis), and CuO–MWCNT mixed network (0.5 wt% MWCNTs, black dots, secondary axis); (b) Seebeck coefficient of the bare CuO layer (orange dot), CuO–MWCNT hybrid composites (blue dots), and CuO–MWCNT mixed networks (black dots, secondary axis) *vs.* MWCNT wt% in the network; (c) mobility (black triangles, primary axis) and charge carrier concentration (blue circles, secondary axis) of the CuO–MWCNT hybrid composites *vs.* MWCNT wt% in the network; (d) power factor of the bare CuO layer (orange dot), CuO–MWCNT hybrid composites (blue dots), and CuO–MWCNT mixed networks (black dots, secondary axis) *vs.* MWCNT wt% in the network.

~2 wt%, followed by a further slight increase for the hybrid CuO–MWCNT composites with MWCNT content above 3 wt% (Fig. 4c, Table 1). However, it should be noted that the changes in the charge carrier concentration were less than one order of magnitude. At the same time, the relative changes in the charge carrier mobility calculated using eqn (2) showed a significant increase of ~1.5–2 times compared with bare CuO when the MWCNT content in the hybrid CuO–MWCNT composites was ~1–2 wt% (Fig. 4c, Table 1). Further increase of the MWCNT wt% resulted in decreased charge carrier mobility, presumably due to the increased scattering at the CuO–MWCNT interfaces (Fig. 4c, Table 1).

The estimated PF of the mixed and hybrid CuO–MWCNT composites is shown in Fig. 4d. The PF of the hybrid CuO–MWCNT composites exceeded the PF of mixed CuO–MWCNT networks by a factor of ~5 and ~50 for the MWCNT wt% of 0.5 and 20 in the mixed networks, respectively (Fig. 4d, Table 1). The PF of the hybrid CuO–MWCNT composites containing ~1–3.5 wt% MWCNTs exceeded the PF of bare CuO by a factor of ~1.5–2. Maximal PF was shown by the hybrid CuO–MWCNT composites with a MWCNT content of ~2 wt%, reaching a maximal value of ~4 μW m^{-1} K^{-2} (Fig. 4d, Table 1). Comparison with other reports showed that the PF reached by the hybrid CuO–MWCNT composites at room temperature exceeded the PF of the CuO–SWCNT composite[30] and CuO[12] nanowires by an order of magnitude (Table 1) and is comparable with the recently reported PF of Sb_2Te_3–MWCNT hybrid networks by our group,[7] while using a significantly less amount of MWCNTs. In addition, it should be noted that the fabrication of few-layer hybrid CuO–MWCNT composites increased their electrical conductance without the degradation of the Seebeck coefficient, which outlines the path for the further improvement of the PF of the hybrid CuO–MWCNT composites. Considering the abundance and safety of CuO for the environment and human health, these results make hybrid CuO–MWCNT composites promising for domestic near-room temperature thermoelectric applications.

Conclusions

Novel CuO–MWCNT hybrid composites with different mass ratios are fabricated by thin metallic Cu layer deposition over the MWCNT network, followed by thermal oxidation of the Cu–MWCNT structure until a complete transition of Cu to CuO. As a result, the MWCNTs were completely incorporated in the nanostructured highly crystalline CuO matrix, which was proved by XRD investigation. Measurements of the Seebeck coefficient and electrical conductivity of the fabricated CuO–MWCNT hybrid composites showed that in contrast with the mixed CuO–MWCNT networks, in the CuO–MWCNT hybrid composites the dominating contributor to the Seebeck coefficient are CuO nanostructures, not MWCNTs. This keeps the Seebeck coefficient at a high level (~500–700 μV K^{-1}) comparable to and even higher than that of the bare CuO nanostructured film (~630 μV K^{-1}), which may be related to the adjustment of charge carrier concentration in the CuO–MWCNT hybrid network due to the electron transfer at the CuO–MWCNT interface. Simultaneously, the fragments of the MWCNTs enclosed between the CuO nanostructures in the CuO–MWCNT hybrid contribute to the increase of the electrical conductance of the CuO–MWCNT hybrid composites, providing highly conductive paths between the CuO nanostructures. Optimal MWCNT concentrations in the CuO–MWCNT hybrid networks, resulting in the increase of PF, were found to be below 5 wt%. Such CuO–MWCNT hybrid nanostructured composites showed an increase in PF by ~2 and ~5–50 times compared to bare CuO and mixed CuO–MWCNT networks, respectively. Moreover, the room-temperature thermoelectric PF of ~4 μW m^{-1} K^{-2} reached by the CuO–MWCNT hybrid nanostructured composites was an order of magnitude higher compared to that of recently reported $[CuO]_{99.9}[SWCNT]_{0.1}$ composites, and comparable with the recently reported PF for Sb_2Te_3–MWCNT hybrid networks while using ~3 times less MWCNTs. These results illustrate promising potential for the application of easily scalable and low-cost CuO–MWCNT hybrid nanostructured composites in domestic applications for low-grade waste heat conversion to electricity.

Author contributions

Conceptualization: J. A. and R. M.; methodology: M. V., R. S., R. M. and J. A.; investigation: M. V., R. S., D. G., E. S., A. K., R. M., and R. L.; visualization: R. S., E. S., A. K., and J. A.; writing – original draft preparation: R. S. and J. A. with contributions from all authors; writing – review and editing: J. A.; supervision: J. A. All authors have read and agreed to the published version of the manuscript.

Data availability

The data presented in this study are available on request from the corresponding author. The data are not publicly available as they are part of ongoing research.

Conflicts of interest

The authors declare no conflict of interest. The funders had no role in the design of the study; in the collection, analyses, or interpretation of data; in writing of the manuscript, or in the decision to publish the results.

Acknowledgements

This work is supported by the ERDF project No. 1.1.1.1/20/A/144. The project was co-financed by REACT-EU to mitigate the effects of the pandemic crisis. R. L. acknowledges the support of Estonian Research Council grants PRG1198 and EAG255.

References

1 J. R. Sootsman, D. Y. Chung and M. G. Kanatzidis, *Angew. Chem., Int. Ed.*, 2009, **48**, 8616–8639.
2 A. J. Minnich, M. S. Dresselhaus, Z. F. Ren and G. Chen, *Energy Environ. Sci.*, 2009, **2**, 466–479.

3 M. L. Lwin, P. Dharmaiah, B. Madavali, C. H. Lee, D. won Shin, G. Song, K. H. Lee and S. J. Hong, *Intermetallics*, 2018, **103**, 23–32.
4 H. Shang, H. Gu, F. Ding and Z. Ren, *Appl. Phys. Lett.*, 2021, **118**, 170503.
5 M. Sattar and W. H. Yeo, *Materials*, 2022, **15**, 4315.
6 Q. Jin, S. Jiang, Y. Zhao, D. Wang, J. Qiu, D. M. Tang, J. Tan, D. M. Sun, P. X. Hou, X. Q. Chen, K. Tai, N. Gao, C. Liu, H. M. Cheng and X. Jiang, *Nat. Mater.*, 2019, **18**, 62–68.
7 J. Andzane, E. Spalva, J. Katkevics, L. Bugovecka, A. Kons, K. Buks and D. Erts, *ACS Appl. Energy Mater.*, 2023, **6**, 10807–10816.
8 K. Buks, J. Andzane, K. Smits, J. Zicans, J. Bitenieks, A. Zarins and D. Erts, *Mater. Today Energy*, 2020, **18**, 100526.
9 L. Ji, *Metal Oxide-Based Thermoelectric Materials*, Elsevier Inc., 2018.
10 Y. Yin, B. Tudu and A. Tiwari, *Vacuum*, 2017, **146**, 356–374.
11 R. Sondors, J. Kosmaca, G. Kunakova, L. Jasulaneca, M. M. Ramma, R. Meija, E. Kauranens, M. Antsov and D. Erts, *Nanomaterials*, 2020, **10**, 1051.
12 D. Zappa, S. Dalola, G. Faglia, E. Comini, M. Ferroni, C. Soldano, V. Ferrari and G. Sberveglieri, *Beilstein J. Nanotechnol.*, 2014, **5**, 927–936.
13 X. Jiang, T. Herricks and Y. Xia, *Nano Lett.*, 2002, **2**, 1333–1338.
14 L. De Los Santos Valladares, D. H. Salinas, A. B. Dominguez, D. A. Najarro, S. I. Khondaker, T. Mitrelias, C. H. W. Barnes, J. A. Aguiar and Y. Majima, *Thin Solid Films*, 2012, **520**, 6368–6374.
15 M. Hübner, C. E. Simion, A. Tomescu-Stănoiu, S. Pokhrel, N. Bârsan and U. Weimar, *Sensor. Actuator. B Chem.*, 2011, **153**, 347–353.
16 M. N. Nahas, A. Jilani and N. Salah, *J. Alloys Compd.*, 2016, **680**, 350–358.
17 Y. Gu, H. Jiang, Z. Ye, N. Sun, X. Kuang, W. Liu, G. Li, X. Song, L. Zhang, W. Bai and X. Tang, *Electron. Mater. Lett.*, 2020, **16**, 61–71.
18 S. R. Mishra and M. Ahmaruzzaman, *Sustain. Mater. Technol.*, 2022, **33**, e00463.
19 K. C. Christoforidis and P. Fornasiero, *ChemCatChem*, 2019, **11**, 368–382.
20 T. Lei, A. Khan, J. Yousaf, A. Deifalla, F. Pan, A. H. Ragab, A. Sayqal, M. Khan, M. Z. Ansari and Y. Khan, *J. Mater. Res. Technol.*, 2023, **24**, 7865–7875.
21 K. Fujimoto, T. Oku, T. Akiyama and A. Suzuki, *J. Phys. Conf. Ser.*, 2013, **433**, 012024.
22 M. Abdel Rafea, A. Eid and W. M. Daoush, *Opt. Mater.*, 2023, **138**, 113643.
23 R. Mulla and M. K. Rabinal, *Mater. Renew. Sustain. Energy*, 2021, **10**, 1–7.
24 J. Andzane, M. V. Katkov, K. Buks, A. Sarakovskis, K. Smits and D. Erts, *Carbon Trends*, 2023, **13**, 100302.
25 K. Buks, J. Andzane, L. Bugovecka, M. V Katkov, K. Smits, O. Starkova, J. Katkevics, A. Bērziņš, L. Brauna, V. Voikiva and D. Erts, *Adv. Mater. Interfaces*, 2022, 2200318.
26 D. V. Sivkov, O. V. Petrova, S. V. Nekipelov, A. S. Vinogradov, R. N. Skandakov, S. I. Isaenko, A. M. Ob'edkov, B. S. Kaverin, I. V. Vilkov, R. I. Korolev and V. N. Sivkov, *Nanomaterials*, 2021, **11**, 2993.
27 R. Sondors, D. Gavars, A. Sarakovskis, A. Kons, K. Buks, D. Erts and J. Andzane, *Mater. Sci. Semicond. Process.*, 2023, **159**, 107391.
28 Y. Cudennec and A. Lecerf, *Solid State Sci.*, 2003, **5**, 1471–1474.
29 J. Yu, T. Huang, Z. Jiang, M. Sun and C. Tang, *Molecules*, 2019, **24**, 441.
30 N. Salah, N. Baghdadi, A. Alshahrie, A. Saeed, A. R. Ansari, A. Memic and K. Koumoto, *J. Eur. Ceram. Soc.*, 2019, **39**, 3307–3314.
31 D. Kim, P. Syers, N. P. Butch, J. Paglione and M. S. Fuhrer, *Nano Lett.*, 2014, **14**, 1701–1706.
32 Y. Yang, D. Xu, Q. Wu and P. Diao, *Sci. Rep.*, 2016, **6**, 35158.